Collisionless Shocks Mediated by Shear-Flow Magnetic Fields in Ultraintense-Laser-Produced Counter-Streaming Plasmas

Jun-Yi Lu, Kai Wang, and Jin-Long Jiao*

Zhejiang Institute of Modern Physics, Institute of Astronomy,

School of Physics, Zhejiang University, Hangzhou 310027, China

(Dated: November 26, 2025)

The formation of ion-Weibel-mediated collisionless shocks (IW-CSs) in ultraintense-laser-produced counter-streaming plasmas is investigated using particle-in-cell simulations. Analysis of the underlying microphysics reveals that a shear-flow ion-Weibel instability generates magnetic fields, which isotropize the incoming flow and mediate shock formation. An analytical expression for the shear-flow magnetic field is derived, and a scaling law relating the magnetic field amplitude to the laser intensity is established. This mechanism reduces the shock formation time and the required laser energy by three and two orders of magnitude, respectively, compared to high-power laser experiments, making it feasible to produce IW-CSs using existing multi-kilojoule, picosecond ultraintense laser facilities.

Collisionless shocks are ubiquitous in a wide range of astrophysical environments, such as active galaxy nuclei, pulsar wind nebulae, and supernovae remnants [1–3]. These shocks contain turbulent magnetic fields, which can produce high-energy cosmic rays with a power-law energy spectrum through the first-order Fermi acceleration mechanism [4–8]. Observable collisionless shocks in the universe are rare, which hinders in-depth studies of their formation, evolution, and role in cosmic ray acceleration. Such shocks have recently been observed in laser-plasma experiments relevant to laboratory astrophysics. These experiments serve as a valuable complement to traditional astronomical observations by reproducing key astrophysical shock phenomena via scaling transformations [9, 10].

Ion-Weibel-mediated collisionless shocks (IW-CSs) are of interest in laboratory astrophysics due to their potential role in generating high-energy cosmic rays [11–15]. Their formation does not require an external magnetic field, relying solely on the self-generated magnetic fields produced by the ion-Weibel instability (IWI). The IWI, a kinetic micro-instability driven by anisotropy in the ion velocity distribution, is readily excited in high-speed counter-streaming plasma systems [16–22]. Through selfgenerated magnetic fields, it deflects ions and converts the kinetic energy of the plasma flow into internal energy, thereby forming collisionless shocks [23, 24]. Generating IW-CSs in the laboratory remains challenging. The most substantial experimental evidence to date was reported by Fiuza et al., who observed this phenomenon in counter-streaming plasmas produced by high-power laser beams at the National Ignition Facility (NIF) [25]. The experiment required a total laser energy of nearly 1 MJ, as shock formation demands large characteristic spatial (centimeter-scale) and temporal (tens of nanoseconds) scales [25–27]. Currently, NIF is the only facility capable of delivering such energy. Although upcoming facilities such as the Laser Megajoule (LMJ) and Shenguang-IV (SG-IV) are designed for megajoule-level output, they

are not yet operational for such experiments. This limitation restricts experimental progress on IW-CSs.

Ultraintense lasers (intensity $> 10^{18} \,\mathrm{W/cm^2}$), which exceed conventional high-power lasers by several orders of magnitude, can generate dense, ultrafast plasma flows. This reduces the spatial and temporal scales needed for shock formation and may lower the required laser energy. Fiuza et al. were among the first to propose a scheme using such lasers to produce collisionless shocks [28, 29]. In their setup, a linearly polarized ultraintense laser interacts with a solid target to form a shock. However, strong laser-driven electron heating leads to mediation by the electron-Weibel instability rather than the IWI. Although the resulting ion deflection resembles that in IW-CSs, the underlying mechanisms are fundamentally different. To suppress electron heating and allow full development of the IWI, Grassi et al. proposed using an obliquely incident S-polarized ultraintense laser [30]. Yet this approach faces experimental challenges: laser pre-pulses, difficult to fully eliminate, typically create a pre-plasma on the target. In such a pre-plasma, even S-polarized light can cause substantial electron heating, preventing the desired conditions from being achieved. More recently, Kuramitsu et al. simulated colliding plasma flows driven by two ultraintense lasers [31]. Using relatively low total energy ($\sim 10 \, \mathrm{J}$), their simulations observed IWI formation but not an IW-CS.

In this Letter, we demonstrate the generation of IW-CSs in counter-streaming plasmas driven by two picosecond-scale ultraintense lasers. Using relativistic PIC simulations, we examine the underlying shock formation physics. Our results reveal an IWI characterized by shear-flow velocity distributions in ultraintense-laser-produced plasmas. This instability generates spatially confined, high-amplitude magnetic fields that mediate shock formation within picoseconds, nearly three orders of magnitude faster than in high-power laser experiments. These shear-flow magnetic fields reduce the required laser

energy, enabling IW-CSs production using existing multikilojoule, picosecond-scale ultraintense laser facilities.

We employ two-dimensional particle-in-cell simulations using the EPOCH code [32] to study the formation of IW-CSs in counter-streaming plasmas. plasmas are generated through the interaction of ultraintense laser pulses with preionized unmagnetized electronproton plasmas. The laser-plasma interaction produces hot electrons that propagate to the target rear and drive high-temperature, high-velocity plasma flows via target normal sheath acceleration (TNSA) mechanism. simulation domain extends from $-500 \,\mu\mathrm{m}$ to $500 \,\mu\mathrm{m}$ in the x-direction and $-150 \,\mu\mathrm{m}$ to $150 \,\mu\mathrm{m}$ in the y-direction. Two identical P-polarized laser pulses with a wavelength of $1 \,\mu \text{m}$ enter from the left and right boundaries along the x-axis. The laser pulse has a temporal profile consisting of a 0.1 ps linear up-ramp (from zero) followed by a 4 ps flat-top region at the peak intensity. For the different cases, the peak intensity ranges from 3.45×10^{19} to $5.52 \times 10^{20} \,\mathrm{W/cm^2}$, corresponding to normalized amplitudes of $a_0 = 5 - 20$. Two symmetric targets are initialized and are uniform along y-direction. For the left target, the pre-plasma extends exponentially from $x = -450 \,\mu\text{m}$ to $-400 \,\mu\text{m}$ with a $7 \,\mu\text{m}$ scale length, reaching $25n_c$ at $x = -400 \,\mu\text{m}$, where it connects to a uniform bulk plasma $(25n_c)$ extending to $x = -150 \,\mu\text{m}$. The reduced bulk density $(25n_c)$ is well below the density of a realistic solid target) is used to avoid numerical heating, but results in higher ion velocities from hole-boring acceleration at the target front. To suppress the artificially high velocities, ions in the region $x < -350 \,\mu\mathrm{m}$ are fixed. Initial electron and ion temperatures are 1 keV and $0.5 \,\mathrm{keV}$, respectively. The grid resolution is $1/12 \mu\mathrm{m}$ (totaling 4.32×10^7 cells). Each cell contains 50 macroelectrons and 50 macro-ions initially. Open boundaries are applied in x-direction, with periodic conditions in ydirection. The real ion-to-electron mass ratio (1836) is used to avoid distortion in shock formation [10, 33].

Ion phase-space signatures confirm the formation of a collisionless shock in ultraintense-laser-produced counter-streaming plasmas. Collisionless shock is a dissipative structure whose formation can be identified by downstream ion thermalization. Fig. 1 shows ion phase-space distributions in counter-streaming plasmas. At the early stage (6 ps), the two plasma flows largely interpenetrate with only minor ion thermalization (Figs. 1a-b), indicating no shock has formed. After a period of evolution (16 ps), the two plasma flows stagnate and thermalize in the central region (Figs. 1c-d), confirming the shock formation. The collisionless nature of the shock is verified by estimating the ion mean free path using $\lambda_{ii} = m_p^2 u_0^4/4\pi e^4 n_e \ln\Lambda$ [34]. With $u_0 \sim 0.1c$, $n_e \sim 10n_c$, and $\ln\Lambda \sim 10$, the resulting $\lambda_{ii} \sim 30\,\mathrm{m}$ far exceeds the shock scale.

The observed collisionless shock is mediated by shear-flow magnetic fields. At the early stage (6 ps), self-

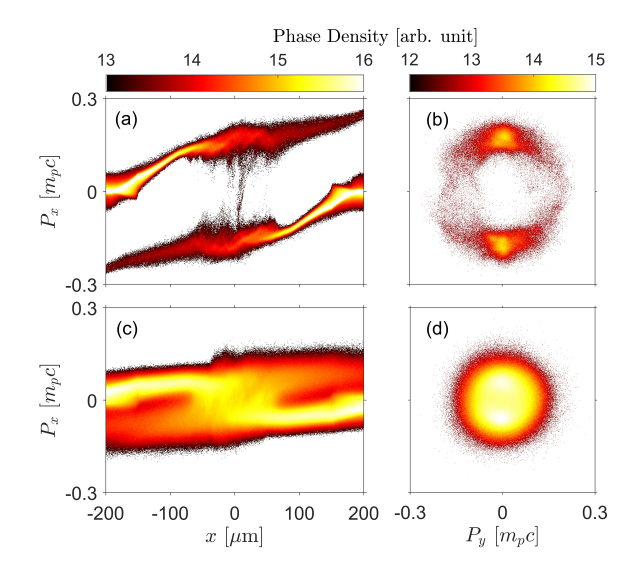


FIG. 1. Ion phase-space density distributions (logarithmic scale) in counter-streaming plasmas produced by ultraintense laser ($a_0 = 10$). (a,c) $x - P_x$ distribution. (b,d) $P_x - P_y$ distribution for ions between $x = -20 \, \mu \text{m}$ and $20 \, \mu \text{m}$. (a,b) and (c,d) show simulation results at 6 ps and 16 ps, respectively.

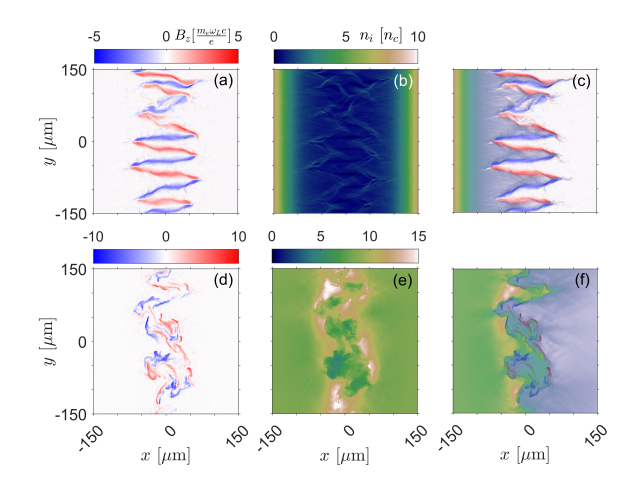


FIG. 2. Self-generated magnetic field and ion density distributions in counter-streaming plasmas produced by ultraintense laser $(a_0 = 10)$. (a,d) Self-generated magnetic field. (b,e) Ion density. (c,f) Magnetic field overlaid with ion density of left plasma flow. (a-c) and (d-f) show simulation results at 6 ps and 16 ps, respectively.

generated magnetic fields and ion density exhibit quasiperiodic filamentary structures (with an average filament width of $\sim 3c/\omega_{pi}$) consistent with the IWI characteristics (Figs. 2a-b). However, unlike classical IWI, the magnetic fields localize specifically within shear layers rather than throughout the entire filament (Fig. 2c). Remarkably, the magnetic field remains localized at the shear interface throughout its evolution, even as the overall structure becomes disordered (Figs. 2d-f). The shearflow magnetic fields, though narrow in width, exhibit

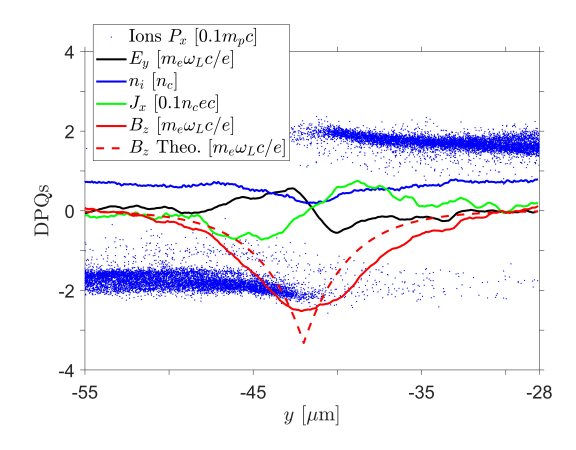


FIG. 3. Profiles of dimensionless physical quantities (DPQs) along the y-direction in a local region ($x = -20 \,\mu\text{m}$ to $15 \,\mu\text{m}$, $y = -55 \,\mu\text{m}$ to $-28 \,\mu\text{m}$) at simulation time $t = 6 \,\text{ps}$.

sufficient strength to deflect ions. Simulations reveal an ion gyroradius of $r_c = m_i u_0 c/Bq \approx 15 \,\mu\mathrm{m}$ ($B \sim 200 \,\mathrm{MG}$ and $u_0 \sim 0.1c$), closely matching the width of shear-flow magnetic field ($\sim 10 \,\mu\mathrm{m}$). This quantitative agreement demonstrates that the shear-flow magnetic field can effectively thermalize ions, thereby enabling shock formation. In addition, electrostatic diagnostics revealed no characteristic signatures of electrostatic collisionless shocks (a localized strong field and periodic oscillations [35, 36]). This rules out an electrostatic instability as the mediating mechanism.

Shear-flow magnetic fields represent a specialized form of the IWI magnetic fields. The IWI magnetic fields originate from net current densities generated by non-uniform ion fluid velocities [12, 33]. In classical IWI scenarios, ion fluid velocities exhibit continuous filamentary structures. In contrast, the shear-flow magnetic field arises from a discontinuous ion fluid velocity [37], as illustrated in Fig. 3 (blue dots). Electrons on either side of the shear interface undergo rapid mixing via the kinetic Kelvin-Helmholtz instability, creating dipolar net current densities at the shear interface (green solid line). This subsequently generates unipolar shear-flow magnetic fields (red solid line) [38, 39]. Under the influence of the shearflow magnetic field, ions on either side of the shear interface tend to separate spatially, resulting in a density gradient (blue solid line). Such density gradients induce electrostatic fields according to the generalized Ohm's law (black solid line). The balance between Lorentz forces and electrostatic forces allows for the stable maintenance of the shear-flow structure.

The one-dimensional expression for shear-flow magnetic fields can be derived through solving the ion current screening (ICS) equation [37]. For relativistic electron temperatures, we define the average relativistic electron

mass as $\bar{\gamma}m_e$, resulting in the ICS equation in CGS units,

$$\frac{c}{4\pi e n_e} \nabla^2 \mathbf{B} - \frac{e}{\eta \bar{\gamma} m_e c} \mathbf{B} + \nabla \times \mathbf{u}_i = 0, \tag{1}$$

where \mathbf{u}_i is ion fluid velocity and η is a kinetic correction factor determined from kinetic simulations. For one-dimensional case, assuming that the discontinuity of shear-flow is at y=0. When y<0, the ion fluid velocity is $\mathbf{u}_i=-u_0\hat{\mathbf{e}}_x$ (along x-direction), when y>0, $\mathbf{u}_i=u_0\hat{\mathbf{e}}_x$. For all positions of $y\neq 0$, Eq. 1 is simplified as,

$$\frac{c}{4\pi e n_e} \frac{\partial^2 B_z}{\partial y^2} - \frac{e B_z}{\eta \bar{\gamma} m_e c} = 0. \tag{2}$$

Eq. 2 only need to be solved over interval $y\in (-\infty,0)$ due to the even symmetry of the shear-flow magnetic field. The general solution of Eq. 2 is $B_z=c_1e^{y/\sqrt{\eta}\bar{\gamma}l_s}+c_2e^{-y/\sqrt{\eta}\bar{\gamma}l_s}$, where $l_s=\sqrt{m_ec^2/4\pi n_ee^2}$ is the skin depth of plasma. c_1 and c_2 are undetermined coefficients, which can be determined by two boundary conditions. The first boundary condition is that as $y\to-\infty$, $B_z=0$, so $c_2=0$. The second boundary condition is that as $y\to0$, electron fluid velocity $u_e=0$, here is $\partial B_z/\partial y=-4\pi n_e e u_0/c$ according to the Ampere's law, so $c_1=-\sqrt{\eta}\bar{\gamma}m_e\omega_{pe}u_0/e$ $(\omega_{pe}=\sqrt{4\pi n_ee^2/m_e}$ is the electron plasma frequency). Finally, the shear-flow magnetic field is

$$B_z = -\sqrt{\eta \bar{\gamma}} \frac{m_e \omega_{pe} u_0}{e} e^{y/\sqrt{\eta \bar{\gamma}} l_s}.$$
 (3)

Eq. 3 (red dashed line) agrees with the simulation results (red solid line) as illustrated in Fig. 3. The parameters $\bar{\gamma} \approx 25$ and $\eta = 10$ are determined from the simulation data. The simulation results exhibit lower amplitudes and broader profiles compared to the predictions of Eq. 3, which can be attributed to minor ion mixing at the shear interface.

The scaling law relating the shear-flow magnetic field to the laser intensity is key to experimental design and can be derived from theoretical analysis and PIC simulations. The maximum field, given by Eq. 3, is

$$B_{z,max} = -\sqrt{\eta \bar{\gamma}} m_e \omega_{pe} u_0 / e \propto n_e^{1/2} u_0 \bar{\gamma}^{1/2}, \qquad (4)$$

The maximum field depends on the electron density n_e , ion fluid velocity u_0 , and the average electron Lorentz factor $\bar{\gamma}$ in the shock region. As n_e is determined by the target design, it is incorporated into a scaling coefficient. The ion fluid velocity scales with the ion sound speed, $u_0 \propto c_s = \sqrt{ZT_e/m_i}$, where the hot electron temperature T_e (generated by the ultraintense laser) scales with the normalized amplitude a_0 according to the established scaling law [40]. This gives $u_0 \propto a_0^{1/2}$. Similarly, $\bar{\gamma} \propto T_e \propto a_0$. Consequently, the scaling law of shear-flow magnetic field and laser intensity takes the form

$$B_{z,max} = \kappa a_0. (5)$$

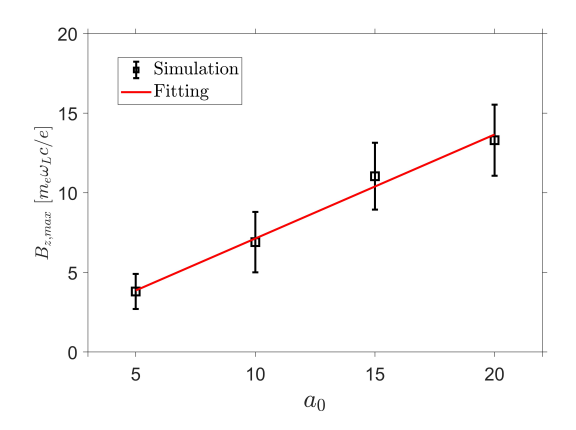


FIG. 4. Scaling law of the shear-flow magnetic field with the normalized laser amplitude. The red solid line represents the least-squares fit. Error bars for the magnetic field data are determined from the statistical variation of local maximum value within the shock region.

The coefficient κ depends on target parameters. For the target configuration used in this work, simulations performed at different laser intensities show that the shearflow magnetic field exhibits a linear dependence on the laser intensity (Fig. 4). A least-squares fit yields a scaling coefficient of $\kappa \approx 0.7 m_e \omega_L c/e$ (ω_L is laser angular frequency).

The shear-flow magnetic fields can reduce the time required for shock formation in ultraintense-laser-produced counter-streaming plasmas. The shock formation time τ is comparable to the ion gyro-period,

$$\tau \sim 2\pi r_c/u_0 = 2\pi m_i c/ZeB_z. \tag{6}$$

By substituting the simulated magnetic field $(B_z \sim 200\,\mathrm{MG})$ from Fig. 2 into Eq. 6, the shock formation time is estimated to be $\tau=3\,\mathrm{ps}$, which closely matches the simulation results. For comparison, in high-power laser experiments conducted by Fiuza et~al. at the NIF [25], shock formation requires several nanoseconds, nearly 3 orders of magnitude longer than that observed in our simulation. This ultrafast shock formation is attributed to the significant enhancement of magnetic field amplitude. In our simulations, all 3 parameters governing the magnetic field amplitude are significantly larger than those in the NIF experiments $(n_e \sim 10^{22}\,\mathrm{cm}^{-3}, u_0 \sim 3 \times 10^4\,\mathrm{km/s}$ and $\bar{\gamma} \sim 25\,\mathrm{for}$ our simulation, $n_e \sim 10^{20}\,\mathrm{cm}^{-3}, u_0 \sim 2 \times 10^3\,\mathrm{km/s}$ and $\bar{\gamma} \sim 1\,\mathrm{for}$ the NIF experiments).

Shear-flow magnetic fields enable collisionless shock formation at substantially reduced temporal and spatial scales, significantly lowering the required laser energy compared to high-power laser experiments. In the Appendix, we present a simulation (transverse width is $50 \, \mu \text{m}$) using a laser energy of $\sim 10 \, \text{kJ}$, a factor of 50 lower

than that used in the NIF experiments (0.455 MJ), in which an IW-CS still forms. The longitudinal scale of the counter-streaming plasmas required for shock formation is determined by ion fluid velocity and shock formation time in shock-region, $L \sim u_0 \tau$. In our simulations, the ultrafast shock formation reduces this longitudinal scale by 2 orders of magnitude compared to the NIF experiments, which significantly increases the shock-region density (by 2 orders of magnitude). The transverse scale required for shock formation is characterized by the width of the shear-flow magnetic field, $w \sim 10\sqrt{\eta \bar{\gamma}} c/\omega_{pe}$ (estimated by the transverse width of $50 \,\mu\text{m}$), in our simulations. The increased shock-region density leads to a transverse scale approximately 2 orders of magnitude smaller than that in the NIF experiments ($w \sim 300c/\omega_{pi}$ [14, 26]). The laser energy required for shock formation scales as $E_L \propto I \tau w^2$ (laser intensity $I \sim 10^{20} \, \mathrm{W/cm^2}$ for our simulation, $I \sim 10^{15} \,\mathrm{W/cm^2}$ for the NIF experiments), indicating that our simulations reduces the required laser energy by nearly 2 orders of magnitude compared to the NIF experiments. Facilities such as OMEGA-EP [41], GEKKO-LFEX [42], SG-II-UP [43], and NIF-ARC [44] already deliver multi-kilojoule, picosecond-scale laser pulses, making them suited for conducting IW-CSs experiments.

In summary, two-dimensional PIC simulations demonstrate that collisionless shocks in picosecond-scale ultraintense-laser-produced counter-streaming plasmas are mediated by shear-flow magnetic fields. We derive a one-dimensional analytical expression for the shear-flow magnetic fields and establish a scaling law relating their amplitude to laser intensity. Key findings reveal that such fields reduce shock formation time by 3 orders of magnitude and lower required laser energy by 2 orders of magnitude compared to the high-power laser experiments

This work is supported by the National Science Foundation of China (No. 12147103).

- * jiao.jl@zju.edu.cn
- R. Blandford, and D. Eichler, Particle acceleration at astrophysical shocks: A theory of cosmic ray origin, Physics Reports 154, 1 (1987).
- [2] T. Piran, The physics of gamma-ray bursts, Rev. Mod. Phys. 76, 1143 (2005).
- [3] E. Waxman, Gamma-ray bursts and collisionless shocks, Plasma Phys. Control. Fusion 48, B137-B151 (2006).
- [4] F. C. Jones, and D. C. Ellison, The plasma physics of shock acceleration, Space Sci. Rev. 58, 259-346 (1991).
- [5] E. Fermi, Galactic Magnetic Fields and the Origin of Cosmic Radiation, Astrophysical Journal 119, 1 (1954).
- [6] D. J. Branch, and C. Wheeler, Supernova Explosions, Berlin: Springer Press, (2017).
- [7] W. Baade, and F. Zwicky, On Super-Novae, Proc. Natl. Acad. Sci. U.S.A. 20 (5), 254-259 (1934).

- [8] K. Koyama, R. Petre, E. Gotthelf et al., Evidence for shock acceleration of high-energy electrons in the supernova remnant SN1006, Nature 378, 255-258 (1995).
- [9] B. A. Remington, R. P. Drake, and D. D. Ryutov, Experimental astrophysics with high power lasers and Z pinches, Rev. Mod. Phys. 78, 755-807 (2006).
- [10] D. D. Ryutov, N. L. Kugland, H. S. Park, C. Plechaty, B. A. Remington, and J. S. Ross, Basic scalings for collisionless-shock experiments in a plasma without preimposed magnetic field, Plasma Phys. Control. Fusion 54, 105021 (2012).
- [11] T. N. Kato, Relativistic Collisionless Shocks in Unmagnetized Electron-Positron Plasmas, Astrophysical Journal 668, 974 (2007).
- [12] A. Spitkovsky, On the Structure of Relativistic Collisionless Shocks in Electron-Ion Plasmas, Astrophysical Journal Letters 673, L39–L42 (2008).
- [13] A. Spitkovsky, Particle Acceleration in Relativistic Collisionless Shocks: Fermi Process at Last?, Astrophysical Journal Letters 682, L5 (2008).
- [14] T. N. Kato, and H. Takabe, Nonrelativistic Collisionless Shocks in Unmagnetized Electron-Ion Plasmas, Astrophysical Journal Letters 681, L93 (2008).
- [15] A. Grassi, and F. Fiuza, Efficient generation of turbulent collisionless shocks in laser-ablated counter-streaming plasmas, Phys. Rev. Research 3, 023124 (2021).
- [16] E. S. Weibel, Spontaneously Growing Transverse Waves in a Plasma Due to an Anisotropic Velocity Distribution, Phys. Rev. Lett. 2, 83 (1959).
- [17] B. D. Fried, Mechanism for Instability of Transverse Plasma Waves, Phys. Fluids 2, 337 (1959).
- [18] J. S. Ross, S. H. Glenzer, P. Amendt et al., Characterizing counter-streaming interpenetrating plasmas relevant to astrophysical collisionless shocks, Phys. Plasmas 19, 056501 (2012).
- [19] W. Fox, G. Fiksel, A. Bhattacharjee, P.-Y. Chang, K. Germaschewski, S. X. Hu, and P. M. Nilson, Phys. Rev. Lett. 111, 225002 (2013).
- [20] D. W. Yuan, Y. T. Li, X. Liu et al., Shockwaves and filaments induced by counter-streaming laser-produced plasmas, High Energy Density Physics 9, 239-242 (2013).
- [21] C. M. Huntington, F. Fiuza, J. S. Ross et al., Observation of magnetic field generation via the Weibel instability in interpenetrating plasma flows, Nature Physics 11(2), 173-176 (2015).
- [22] M. J.-E. Manuel, M. B. P. Adams, S. Ghosh et al., Experimental evidence of early-time saturation of the ion-Weibel instability in counterstreaming plasmas of CH, Al, and Cu, Phys. Rev. E 106, 055205 (2022).
- [23] S. S. Moiseev, and R. Z. Sagdeev, Collisionless shock waves in a plasma in a weak magnetic field, J. Nucl. Energy, Part C Plasma Phys. 5, 43-47 (1963).
- [24] M. V. Medvedev, and A. Loeb, Generation of Magnetic Fields in the Relativistic Shock of Gamma-Ray Burst Sources, Astrophysical Journal 526, 697-706 (1999).
- [25] F. Fiuza, G. F. Swadling, A. Grassi et al., Electron acceleration in laboratory-produced turbulent collisionless shocks, Nature Physics 16, 916-920 (2020).
- [26] H.-S. Park, C. M. Huntington, F. Fiuza et al., Collisionless shock experiments with lasers and observation of Weibel instabilities, Phys. Plasmas 22, 056311 (2015).
- [27] J. S. Ross, D. P. Higginson, D. Ryutov et al., Transition from collisional to collisionless regimes in interpenetrating plasma flows on the National Ignition Facility, Phys.

- Rev. Lett. 118, 185003 (2017).
- [28] F. Fiuza, R. A. Fonseca, J. Tonge, W. B. Mori, and L. O. Silva, Weibel-Instability-Mediated Collisionless Shocks in the Laboratory with Ultraintense Lasers, Phys. Rev. Lett. 108, 235004 (2012).
- [29] C. Ruyer, L. Gremillet, and G. Bonnaud, Weibel-mediated collisionless shocks in laser-irradiated dense plasmas: Prevailing role of the electrons in generating the field fluctuations, Phys. Plasmas 22, 082107 (2015).
- [30] A. Grassi, M. Grech, F. Amiranoff, A. Macchi, and C. Riconda, Radiation-pressure-driven ion Weibel instability and collisionless shocks, Phys. Rev. E 96, 033204 (2017).
- [31] Y. Kuramitsu, Y. Matsumoto, and T. Amano, Nonlinear evolution of the Weibel instability with relativistic laser pulses, Phys. Plasmas 30, 032109 (2023).
- [32] T. D. Arber, K. Bennett, C. S. Brady et al., Contemporary particle-in-cell approach to laser-plasma modelling, Plasma Phys. Control. Fusion 57, 113001 (2015).
- [33] C. Ruyer, L. Gremillet, G. Bonnaud, and C. Riconda, Analytical Predictions of Field and Plasma Dynamics during Nonlinear Weibel-Mediated Flow Collisions, Phys. Rev. Lett. 117, 065001 (2016).
- [34] L. Spitzer, Physics of Fully Ionized Gases, Wiley-Interscience: New York (1962).
- [35] D. A. Tidman, N. A. Krall, Shock Waves in Collisionless Plasmas, Wiley-Interscience: New York (1971).
- [36] J. L. Jiao, S. K. He, H. B. Zhuo et al., Experimental Observation of Ion–Ion Acoustic Instability Associated with Collisionless Shocks in Laser-produced Plasmas, Astrophysical Journal Letters 883, L37 (2019).
- [37] J. L. Jiao, Ion Current Screening Modeling of the Ion-Weibel Instability, Astrophysical Journal 924, 89 (2022).
- [38] E. P. Alves, T. Grismayer, S. F. Martins, F. Fiuza, R. A. Fonseca, and L. O. Silva, Large-scale magnetic field generation via the kinetic kelvin-helmholtz instability in unmagnetized scenarios, Astrophysical Journal Letters 746, L14 (2012).
- [39] T. Grismayer, E. P. Alves, R. A. Fonseca1, and L. O. Silva, dc-Magnetic-Field Generation in Unmagnetized Shear Flows, Phys. Rev. Lett. 111, 015005 (2013).
- [40] S. C. Wilks, W. L. Kruer, M. Tabak, and A. B. Langdon, Absorption of ultra-intense laser pulses, Phys. Rev. Lett. 69, 9 (1992).
- [41] J. H. Kelly, L. J. Waxer, V. Bagnoud et al., OMEGA-EP: Highenergy petawatt capability for the OMEGA laser facility, Journal de Physique IV (Proceedings) 133, 75-80 (2006)
- [42] N. Miyanaga, H. Azechi, K. A. Tanaka et al., 10-kJ PW laser for the FIREX-I program, Journal de Physique IV (Proceedings) 133, 81-87 (2006).
- [43] J. Q. Zhu, J. Zhu, X. C. Li et al., Status and development of highpower laser facilities at the NLHPLP, High Power Laser Science and Engineering 6, e55 (2018).
- [44] C. P. J. Barty, M. Key, J. Britten et al., An overview of LLNL highenergy short-pulse technology for advanced radiography of laser fusion experiments, Nuclear Fusion 44(12), S266-S275 (2004).

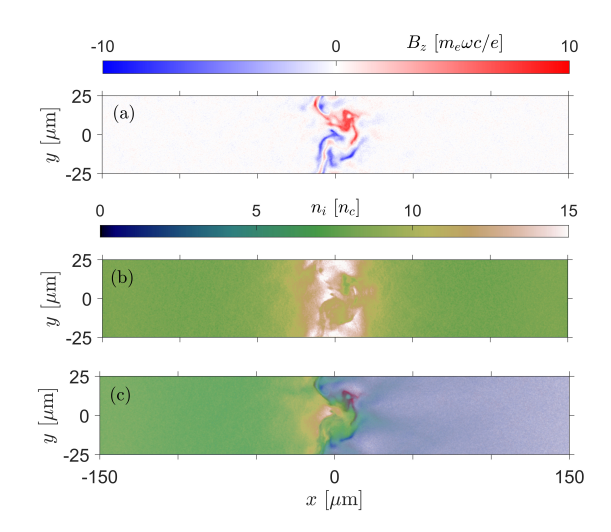


FIG. 5. Ultraintense-laser-produced collisionless shock in a reduced transverse scale simulation (at 16 ps). (a) Self-generated magnetic field. (b) Ion density. (c) Magnetic field overlaid with ion density of left plasma flow.

Appendix: Simulation with reduced transverse scale - A simulation case with lower laser energy was carried out. This case reduced the simulation transverse scale to $50\,\mu\mathrm{m}$, other parameters are the same as the Fig. 2. The laser energy on each target is $E_L = I\tau\pi r^2$, where laser intensity $I = 1.38 \times 10^{20}\,\mathrm{W/cm^2}$, radius of laser focus spot is $r = 25\,\mu\mathrm{m}$, laser duration is $\tau = 4\,\mathrm{ps}$. So $E_L = 10.8\,\mathrm{kJ}$. Fig. 5 shows the formation of both the shear-flow magnetic fields and the IW-CS, consistent with the results presented in Fig. 2.